Application of Mechanoluminescence for the Dynamic Visualization of an Alumina Fracture

Ji Sik Kim*

Abstract

The propagation of cracks was quantitatively analyzed in Al_2O_3 ceramic using the mechanoluminescence (ML) of $SrAl_2O_4$:Eu,Dy. The bridging zones behind the crack tip were clearly detected in the crack path of Al_2O_3 within a realistic time frame. The magnitudes and shapes of the bridging stress distributions changed with the advancing cracks. They continued to change with the change in the applied load even after the cessation of crack propagation. Effective toughening then commenced, and the applied stress intensity factors dramatically increased up to ~50 MPa$\sqrt{m}$. The expected K_{Tip} values based on the instantaneous bridging stress distributions obtained from the ML observations deviated greatly from those obtained from the measurement using the conventional crack tip lengths; rather, they support the results obtained when bridging tips were used in the quasidynamic crack propagations.

Keywords: mechanoluminescence, quasidynamic fracture, crack propagation, grain bridging

1. Introduction

It is generally known that non-transforming monolithic polycrystalline ceramic materials exhibit R-curve behavior due to the grain bridging in the crack wake region, which has been extensively investigated for several structural ceramics, such as Si_3N_4, SiC, and Al_2O_3 [1-3]. Using various specimens, such as a double cantilever beam (DCB), double torsion (DT), compact tension (CT), and a single-edge notched bar (SENB), the so-called long-crack R-curve behaviors were measured under subcritical conditions [4-7]. In all these specimens, the precise tracking of a propagating crack tip was the most significant experimental concern. As only the traveling-optical-microscope and loading-unloading techniques have been widely utilized to detect stationary cracks under quasistatic conditions, however, the crack length value is obtained through the conventional R-curve measurements in various specimen systems for structural ceramic materials. Therefore, a crack in the conventional test specimens has a duality in its dimensional scale. The length spans over 10^{-2} m, but the crack tip opening the displacement around the tip will be in the order of 10^{-9} m, or even less. This will hamper the instantaneous determination of the correct length of a crack because it is advancing at a high rate. Most experimental fracture analyses of structural ceramics have been implemented under conditions of quasistatic crack propagation manipulated artificially.

Even though several high-cost, cumbersome methodologies, such as laser photoelasticity, laser ultrasound, Raman spectroscopy, X-ray analysis, electrical-resistance measurement, and a strain gauge (or wire) attachment technique [8-12], have been utilized for the effective detection of cracks accompanying a stress field, it should be noted that they are all indirect methods. All these attempts are different from direct visualization and also require complicated experiment procedures even for the purpose of obtaining simple results. Therefore, no attempts have been made to visualize in-situ crack propagation under quasidynamic conditions, or to obtain quasidynamic R-curves, until the mechanoluminescence (ML) technique was employed [13-17]. In the previous research, crack propagation was successfully analyzed in association with the bridging behavior around the crack wake for monolithic, polycrystalline ceramics under quasidynamic conditions [13-17]. The stress intensity factors, however, increased dramatically up to several hundreds MPa$\sqrt{m}$ in all the ceramics, which is unrealistically high compared to the conventional qua-

Manuscript Received February 12, 2010; Revised February 23, 2010; Accepted for publication March 4, 2010
This study was supported by a Korea Research Foundation grant (KRF-313-2007-2-D00336)
* Member, KIDS
Corresponding author : Ji Sik Kim
School of Nano & Materials Science Engineering, Kyungpook National University, Kyeongbuk, 742-711, South Korea
E-mail: Jisikkim@knu.ac.kr **Tel**: +82-45-530-1413 **Fax**: +82-45-530-1418

sistatic R-curves.

In this research, so that the problem could be analyzed systematically, the focus was placed on visualizing the evolution of the crack accompanying the wake region under a relatively slower loading condition compared to those in the previous experiments, in a compact-tension-(CT)-type specimen made of Al_2O_3 ceramic, using the ML technique, which made it possible to determine the bridging evolution more quantitatively due to the slow crack propagation. The systematic application of the ML technique to ceramics exhibiting R-curve behavior due to grain bridging, such as Al_2O_3 in addition to the previous Si_3N_4 and SiC ceramics [18], would also pave the way for a more quantitative understanding of the toughening mechanism and stress intensity factor by comparing the instantaneous macroscale observations of Si_3N_4, SiC, and Al2O3 ceramics.

ML is a photoemission from some special materials, such as $SrAl_2O_4$:Eu,Dy phosphors, due to applied mechanical stimulation. These mechanical actions can include friction, pressure, bending, erasing or rubbing, and shocking and fracture. The mechanism of ML can be accounted for parallel to long phosphorescence, thermally stimulated luminescence, and photostimulated luminescence, all of which are associated with a trap-involved process [16]. The ML phenomenon arising in $SrAl_2O_4$:Eu,Dy phosphors was utilized as a stress indicator because the phosphors were prepared in bulky epoxy mixture forms [14]. More recently, some additional pragmatic usages of $SrAl_2O_4$:Eu,Dy phosphors (e.g., as sintered ceramics [15], paints [13], and thin films [16]) were introduced in an attempt to achieve an efficient stress indicator. These new developments can be very powerful from a practical point of view when used for conventional mechanical testing as a stress or crack indicator. As a testing means, CT-type specimen systems were employed in association with the above-described ML techniques so that relatively fast crack propagation and its corresponding wake development around the crack surface could be visualized in terms of ML [13]. Therefore, the ML technology is not only a versatile tool for the study of fracture mechanism but also has a potential for use in the low-cost safety diagnosis of structural components or in the visualization of microelectromechanical system operations.

2. Experiment Procedure

ML paint was prepared by mixing epoxy resin with 15 vol% $SrAl_2O_4$:Eu,Dy powder, which was then either evenly plastered or sprayed on the specimen surface. Hard epoxy resins with a Young's modulus of 2.6 were prepared. The Al_2O_3 samples purchased from Cerakor Co., Ltd. were sintered in a disc shape, close to the final dimension of a disc-type CT specimen (Fig. 1), consistent with the ASTM E399 specifications [18]. An acute notch tip was introduced into the CT specimen using a very sharp blade with a thickness of 35 μm, to produce a crack initiation point. The resulting notch tip radius was about 50 μm. The CT specimen was then coated with ML paint. The thickness of the paint layer was about 100 μm. The painted CT specimen was placed on an Instron machine equipped with a specially designed CT-type loading stage. The specimen was exposed to a high-intensity 365-nm UV light for 5 min and was then aged in the dark for 1 min to allow the long phosphorescence to relax to a reasonable level before loading. The crosshead speed was 0.5 mm/min, equivalent to several MPa$\sqrt{m}$/sec, which is much faster than the conventional values (the most frequently used values are several μm/min or, at best, 100 μm/min) in R-curve measurements with a long-crack system, such as compact tension (CT), double torsion, double cantilever beam, and single-edge notched bar. The entire crack path, covering the crack tip process zone and wake area, was then photographed on a macro scale at a frame speed of 8,000 frame/sec, using a high-speed imaging system. The use of a multichannel datalink (MCDL) made it possible to record the load data from a piezoelectric load cell for each image frame, thus assuring perfect coincidence between the recorded images and the load data, with no time delay, allowing the calculation of the instantaneous value of the stress intensity factor. Scanning electron microscopy (SEM) was also used to investigate the facture

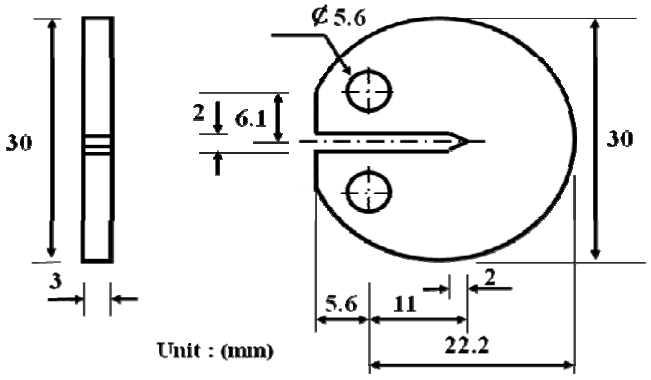

Fig. 1. Schematic drawing of a disc-type compact tension specimen showing the dimension and shape.

surfaces of the alumina samples after the compact tension tests.

3. Results

Fig. 2 shows the typical series of real-time ML images representing crack propagation for about 1 msec in the Al_2O_3 CT specimen loaded at a crosshead speed of 0.5 mm/min. The quasidynamic fracture process in alumina arises via two distinct steps, as can be seen in Fig. 2. The first step represents the typical crack propagation process. About-2.4-mm-long cracks were initiated abruptly from the machined notch tip in alumina, indicating that a crack wake was created behind the crack tip. As the frame speed was 8,000 frame/sec, each frame was photographed for about 125 μsec. It appeared that the initial crack propagation arose within a period considerably shorter than 125 μsec. This first crack speed was quite high (approximately 0.3 m/sec) compared to quasistatic crack propagation (typically 10^{-3}~10^{-2} m/sec). As this speed level did not reach the dynamic fracture regime, however, a dynamic effect can be ruled out. This observation was consistently confirmed in all the ML experiments where loading rates that give rise to realistic, catastrophic crack speeds (quasidynamic condition) were adopted. After the crack initiation, the crack further propagated for 8.7 mm in the next four frames, approaching the edge of the specimen, indicating that the specimen was divided by the crack but was not separated by it. This is a well-known R-curve characteristic, as shown in renotching [19] and post-fracture tensile tests [20].

The major interest in the present research, however, lay in the subsequent events. These authors focused their attention on the brighter ML behind the crack tip, which moved towards the crack front, eventually reaching it. A similar type of fracture has already been reported by these authors in alumina as well as in SiC and Si_3N_4, under similar quasidynamic conditions [13]. This phenomenon is defined by the second step of the quasidynamic fracture process in the previous results. To investigate the second step in a more systematic manner, the ML in Fig. 2(a) was converted to the relative stress in Fig. 2(b) by reading the RGB value of the bitmap file of each image in Fig. 2(a). The line integration of the RGB (red, green, blue) value along the vertical direction at a certain location on the horizontal axis yielded a relative value for the closure (bridging) stress acting on the crack surface at that location. As it is well known that the extent of ML increases with the stress rate, and that the relationship between the two is almost linear, such simple integration of ML is reasonable in the calculation of the relative stress field [21]. The result from the first frame, where no crack was used as a background, should be subtracted from all the other frames. Fig. 2(b) shows that the shape of the bridging stress rate distribution gradually changed in the crack wake region, thereby allowing the accumulative bridging stress distribution values in alumina to be obtained, as shown in Fig. 2(c). The SEM micrograph also shows the trace of the grain interface bridging in all the areas of the specimens. As can be seen in Fig. 3, the sizes of the grains are within the range of several tens of microme-

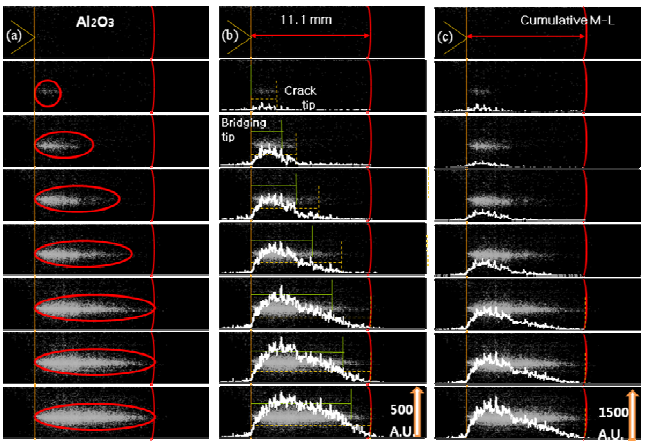

Fig. 2. (a) Sequence of high-speed ML images at a frame speed of 8,000 frame/sec for 125 μsec in Al_2O_3, along with the (b) bridging stress rate and (c) cumulative-stress distribution converted from ML. The instantaneous locations of the crack and bridging tips are also marked.

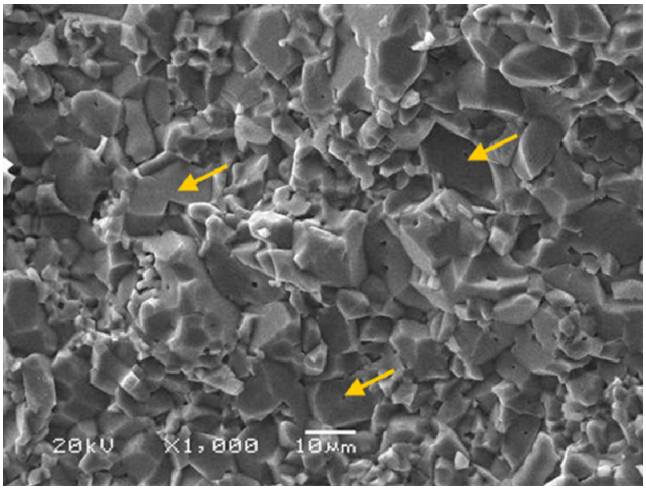

Fig. 3. SEM micrograph showing the intergranular fractures in Al_2O_3.

ters, which is slightly small for conventional bridging in alumina. All the fractures, however, took place in an intergranular way. The population of the grains cleaved in a transgranular way was very small compared with the population of the grains cleaved in an intergranular way. There is no doubt that grain interface bridging took place in all the regions of the specimens. Therefore, based on the results of the M-L visualizations and the SEM micrographs, it can be concluded that the conventional ceramic fracture related with grain bridging shows the separated two-step fractures, including crack propagation and bridging breakage.

4. Discussion

To these authors' knowledge, no reports dealing with the direct estimation of bridging stress distribution as a function of the distance behind the crack tip for a propagating crack have yet been made, even though bridging stress distribution has been directly measured with respect to COD using the well-known renotching and post-fracture tensile tests [19,20]. As far as bridging stress distribution as a function of COD is concerned, a strain-softening behavior expressed by a simple power law function has been verified. On the other hand, several indirect methods for obtaining bridging stress distribution as a function of the distance behind the crack tip have been developed, based on regression fitting, using an R-curve [21], compliance [22], and COD data.23 These indirect methods obliged these authors to incorporate the following two unrealistic assumptions: that the bridging stress distribution should be expressed by the power law function with respect to the distance behind the crack tip, and that it is assumed to have a constant profile irrespective of the crack propagation. These assumptions have also been made in almost all the theoretical modelings of bridging stress [24]. The real features of bridging stress distribution observed in Al_2O_3, as shown in Fig. 2(b), and in the previous results in Si_3N_4 and SiC are in sharp contrast to the aforementioned assumptions [13]. The actual bridging stress distribution is of a nonpower law form, and both its magnitude and shape vary as the crack propagates. This implies crack resistance. As such, the stress intensity factor and the existing R-curve concept are strongly affected by the bridging breakage process and not by crack propagation.

Now that the two-step process for the dynamic fracture of Al_2O_3 has been considered, the quasidynamic R-curves should be estimated. Taking the instantaneous crack length as crack tip and load values, as shown in Fig. 2(b), the instantaneous stress intensity factors can be depicted as functions of the ratio of crack length to specimen width, as can be seen in Fig. 4. The quasidynamic R-curves were found to be within the range of 5-50 MPa$\sqrt{m}$. They had a downward convex shape, which is quite common in the case of CT-type R-curve measurements [25]. It should be noted that the stress intensity factors increased dramatically up to 50 MPa$\sqrt{m}$, which is extraordinarily high compared to those of the conventional quasistatic R-curves. It has been argued that the unrealistic value of the stress intensity factor is associated with the relative size of the specimen compared to the bridging zone size [25]. Even if such a specimen dimension effect were considered, however, 50 MPa$\sqrt{m}$ would still be too high for the conventional Al_2O_3. It appears that the increase not only in the specimen dimension effect but also in the crack length through the more accurate detection of the crack tip owing to the ML technique is responsible for the unrealistic value of the stress intensity factor. It is clearly noted, in contrast, that taking the bridging tip as an instantaneous crack length in Fig. 2(b) will yield the reasonable increase of the K_{Tip} value and of the R-curve behavior, as can be seen in Fig. 4. These results also suggest the decisive role of the bridging breakage process during fracture in considering the K_{Tip} value in the mechanical aspects with non-transforming monolithic polycrystalline ceramics.

To prove the aforementioned hypothesis, the R-curve was computed based on Green's function [25], as follows. It

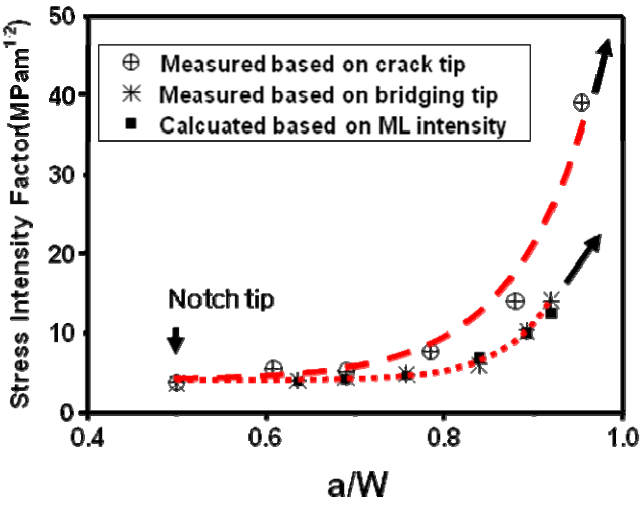

Fig. 4. Experimental quasidynamic R-curves obtained from the crack and bridging tip, and the values obtained from the calculation based on Green's function in Al_2O_3.

is generally known that the crack tip shielding effect can be written in terms of stress intensity balance, such that

$$K_{Tip} = K_{app} - \Delta K \quad (1)$$

where K_{Tip} is the stress intensity factor at the crack tip, which acts as the major driving force for crack growth, K_{app} the applied stress intensity factor, and ΔK the contribution from wake shielding. Provided that the crack is in the critical (equilibrium) state, an alternative expression is also available, such that

$$K_R = K_O + \Delta K \quad (2)$$

where KR is the crack resistance (R-curve), KO the intrinsic toughness of the material without any wake effect, and ΔK the contribution from wake shielding. The directly measured relative bridging stress distributions were incorporated as P(x)s in Green's function.

$$\Delta K(\Delta C) = 2\sqrt{(C_O + \Delta C)/\pi} \int_0^{\Delta C} \frac{P(x)}{\sqrt{(C_O + \Delta C)^2 - (C_O + \Delta C - x)^2}} dx \quad (3)$$

where C_O is the initial notch length and ΔC the crack extension, x the distance behind the crack tip, and $P(x)$ the bridging stress distribution. In most cases, this calculation has been implemented under the assumption that the $P(x)$ function is independent of the specimen and the crack geometry, as well as of the loading conditions. Otherwise, a correction factor (= weight factor), which is a function of x, ΔC, and W (specimen width), will be included in the integrand term of equation (3) [29-31]. In this report, Green's function was employed without any correction term, but the final calculation results of K_{Tip} are in very good agreement with the measurement values obtained from the bridging breakage process, as can be seen in Fig. 4. The calculated R-curves, designated by the solid box symbols, also exhibit the downward convex shape, and the value of the stress intensity factor approached 15, which is quite reasonable in alumina. Therefore, the prominent mismatch between the measurement value obtained based on the crack tip and the calculated R-curves in alumina mainly seems to be the result of the overestimated crack length through the more accurate detection of the crack tip owing to the ML technique.

5. Summary

The ML technique enabled the macroscale visualization of crack propagations together with the bridging zones (crack wakes) behind the crack tip in Al_2O_3 in a more realistic time frame by simulating an actual catastrophic fracture, escaping from quasistatic conditions. Mechanoluminescence made it possible to detect relatively fast (0.3 m/sec) crack propagation, thereby realizing the so-called "quasidynamic R-curves" in Al_2O_3.

Systematic observations of crack propagation and of the bridging breakage process as well as of quasidynamic R-curves were successfully done during catastrophic fracture. Effective toughening then commenced, and the applied stress intensity factors increased dramatically to 50 $MPa\sqrt{m}$, which was too high for the conventional Al_2O_3. The R-curve behavior obtained from the ML observation based on the bridging breakage process, however, was in very good agreement with those predicted by Green's function.

References

[1] J.J. Kruzic , R.M. Cannon, J.W. Ager III, and R.O. Ritchie, *Acta Mater*. **53** 2595 (2005).
[2] C.J. Gilbert, and R.O. Ritchie, *Acta Mater*. **46** 609 (1998).
[3] R.D. Geraghity, J.C. Hay, and K.W. White, *Acta Mater*. **47** 1345 (1999).
[4] M.E. Ebrahimi, Chevalier, and Fantozzi, *J. Eur. Ceram. Soc*. **23** 943 (2003).
[5] H. Ichimaru, and Pezzotti, *Mater. Sci. Eng. A* **326** 261 (2002).
[6] R.E. Grimes, G.P. Kelkar, and L. Guazzone, K.W. White, *J. Am. Ceram. Soc*. **73** 1399 (1990).
[7] R.W. Steinbrech, A. Reichl, and W. Schaarwächter, *J. Am. Ceram. Soc*. **73** 2009 (1990).
[8] A.J. Rosakis, O. Samudrala, and D. Coker, *Science* **284** 1337 (1999).
[9] Q. Shan, and R.J. Dewhurst, *Appl. Phys. Lett*. **62** 2649 (1993).
[10] H. Nakano, and S. Nagai, *Jpn J. Appl. Phys*. **32** 2540 (1993).
[11] T. Yoshimura, N. Akiyama, M. Yoshida, and T. Kobayashi, *Int. J. Jpn Soc. Prec. Eng*. **29** 168 (1995).
[12] B. Zhang, J.B. Li, Y. Deng, Z.D. Guan, *Smart mater. Struct*. **10** 846 (2001).
[13] J.S. Kim, Y.N. Kwon, N. Shin, and K.S. Sohn, *Acta Mater*. **53** 4337 (2005).
[14] K.S. Sohn, S.Y. Seo, Y.N. Kwon, and H.D. Park, *J. Am. Ce-*

ram. Soc. **85**, 712 (2002).
[15] J.S. Kim, Y.N. Kwon, N. Shin, and K.S. Sohn, *Acta Mater*. **51**, 6437 (2003).
[16] K.S. Sohn, D.H. Park, and J.S. Kim, *J. Electrochem Soc*. **152**, H161 (2005)
[17] J. S. Kim, K. Kibble, M. Stanford, Y. N. Kwon, K.-S. Sohn, *Met. Mat. Int*. **14**, 165 (2008).
[18] *ASTM Standard Test Method for Plane-Strain Fracture Toughness of Metallic Materials*, ASTM E399-83.
[19] X.Z. Hu, and F.H. Wittmann, *J. Mater. Civil Eng*. **2** 15 (1990).
[20] J.C. Hay, and K.W. White, *Acta Metal. Mater*. **40** 3017 (1992).
[21] T. Fett, D. Munz, and G. Thun, J. Am. Ceram. Soc. 78 949 (1995).
[22] X.Z. Hu, E.H. Luts, and M. Swain, *J. Am. Ceram. Soc*. **74** 1828 (1991).
[23] J. Rödel, J. Kelly, and B.R. Lawn, *J. Am. Ceram. Soc*. **73** 3313 (1990).
[24] S.J. Bennison, and B.R. Lawn. *Acta Mater*. **37** 2659 (1989).

[Parts of this work were presented in Proceedings of IMID 2009.]